Australian National University

# Thermal Model of a Solar Thermochemical Reactor for Metal Oxide Reduction

Bo Wang, Lifeng Li, Johannes Pottas, Roman Bader, Peter B. Kreider, Vincent M. Wheeler, and Wojciech Lipiński

Solar Thermal Group
College of Engineering & Computer Science
The Australian National University

Asia–Pacific Solar Research Conference
6th December 2018

# Introduction

| Material | Energy storage mechanism | Temperature | Power cycle | Energy storage density |
|---|---|---|---|---|
| Molten salts [1] | Sensible heat | < 900 K | Rankine/$SCO_2$ Brayton | ~ 1.5 GJ $m^{-3}$ |
| Manganese oxides [2] | Thermochemical energy | 1400–1800 K | Combined Brayton–Rankine | ~ 3 GJ $m^{-3}$ |

A transient thermal model is developed to study the thermal performance of the high-temperature solar thermochemical reduction reactor.

**Objectives**

- Safety
  - Peak temperature
  - Peak thermal stress
- Solar-to-thermochemical efficiency

$$\eta_{\text{s-t}} = \frac{\dot{m}\Delta h_{\text{p}}}{C \cdot A \cdot \text{DNI}}$$

- Effect of incident radiation directionality

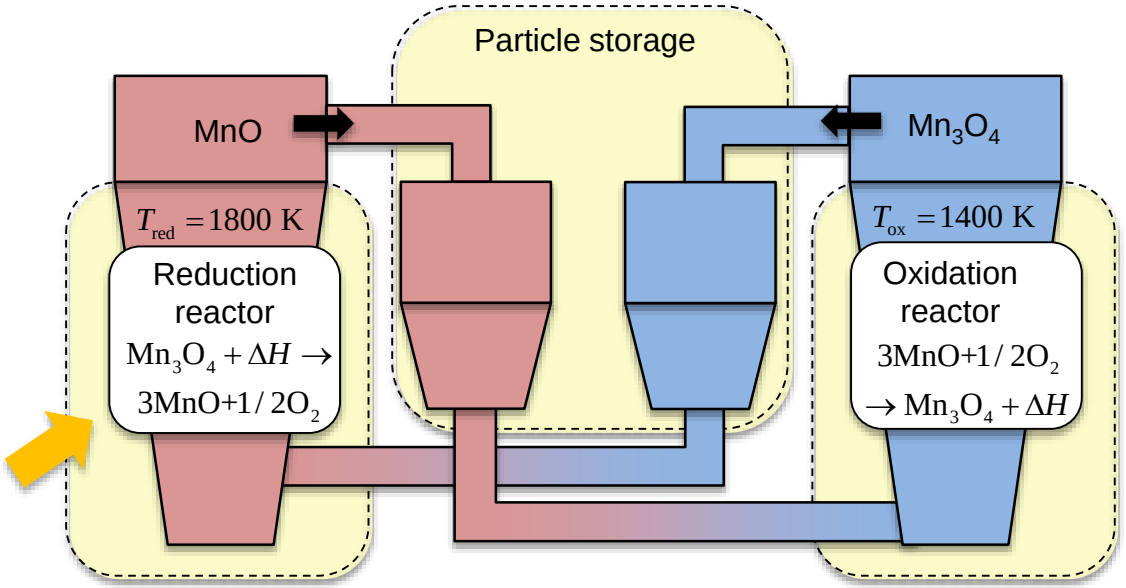


Fig 1. Schematic of a high-temperature solar thermochemical energy storage system for dispatchable and efficient power generation.


Reference:
[1] Pilkington Solar International GmbH, Survey of thermal storage for parabolic trough power plants, NREL, Report, NREL/SR-550-27925 (2000).
[2] A. Gil, M. Medrano, I. Martorell, A. Lázaro, P. Dolado, B. Zalba, L. F. Cabeza, State of the art on high temperature thermal energy storage for concentrated power generation. part 1—concepts, materials and modellization, Renewable Sustainable Energy Review 14 (1) (2010) 31–55.

# Problem statement

**Reactor geometry**
- Absorptive reactor tube (SiC)
- Diffuse reflective cavity (alumina)
- Compound parabolic concentrator (CPC)

**Operation**
- Incident radiation 2.4 kW
- Concentration ratio ~ 3000 suns
- No flow at start-up

**Assumptions**
- Convection loss in cavity neglected
- Pseudo 3-D conduction in insulation layers
- Reactive flow approximated as heat sink at constant temperature

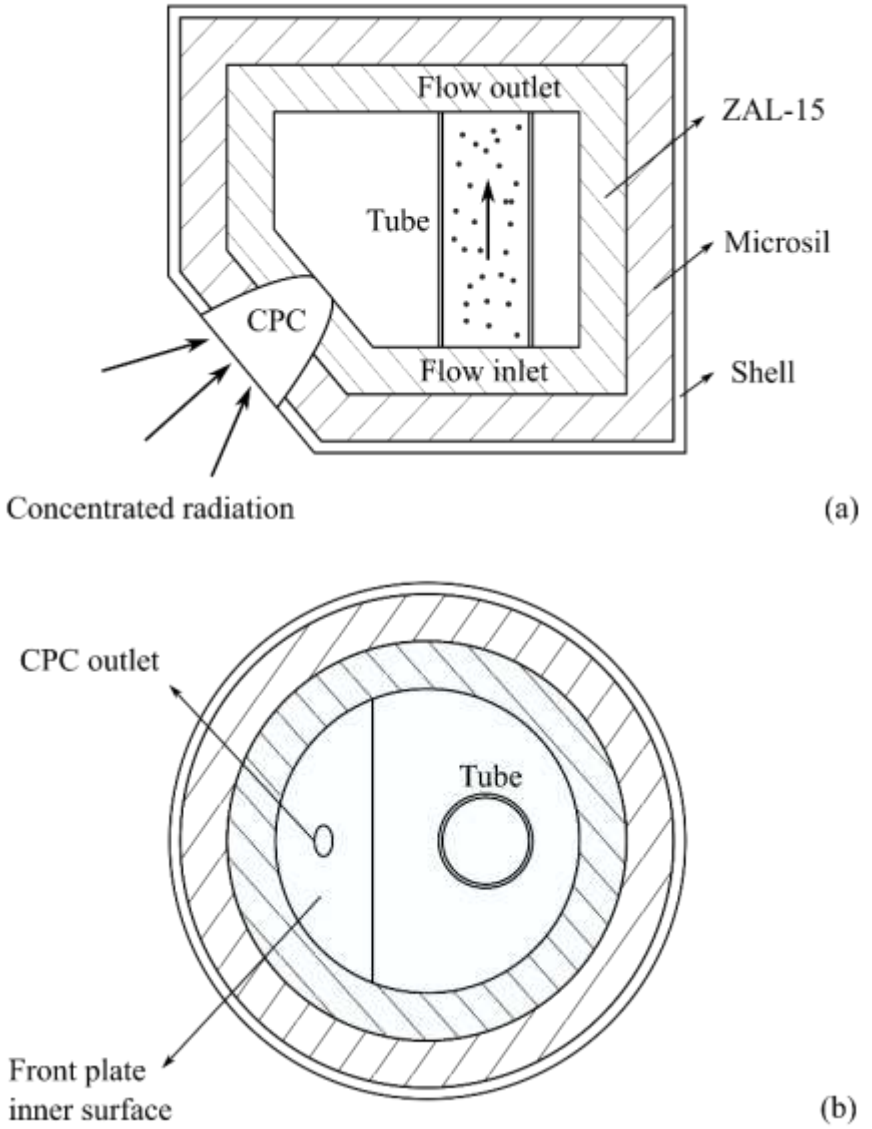


Fig 2. Schematic of the proposed reactor (a) side view, (b) top view.

# Governing equations

- Energy conservation

$$\rho c_p \frac{\partial T}{\partial t} = -\nabla \cdot \mathbf{q}''_{\text{cond}} = \nabla \cdot k_{\text{cond}} \nabla T$$

- Thermochemistry

$$\mathrm{Mn_3O_4} \rightarrow 3\mathrm{MnO} + \frac{1}{2}\mathrm{O_2}$$

$$\dot{n}_{\mathrm{N_2,inlet}} = \frac{\dot{m}_{\mathrm{N_2,inlet}}}{M_{\mathrm{N_2}}} = \frac{\rho_{\mathrm{N_2}} A_{\text{tube}} u_{\text{mb}}}{M_{\mathrm{N_2}}}$$

$$\dot{n}_{\mathrm{O_2}} = \frac{1}{2}\dot{n}_{\text{p}}$$

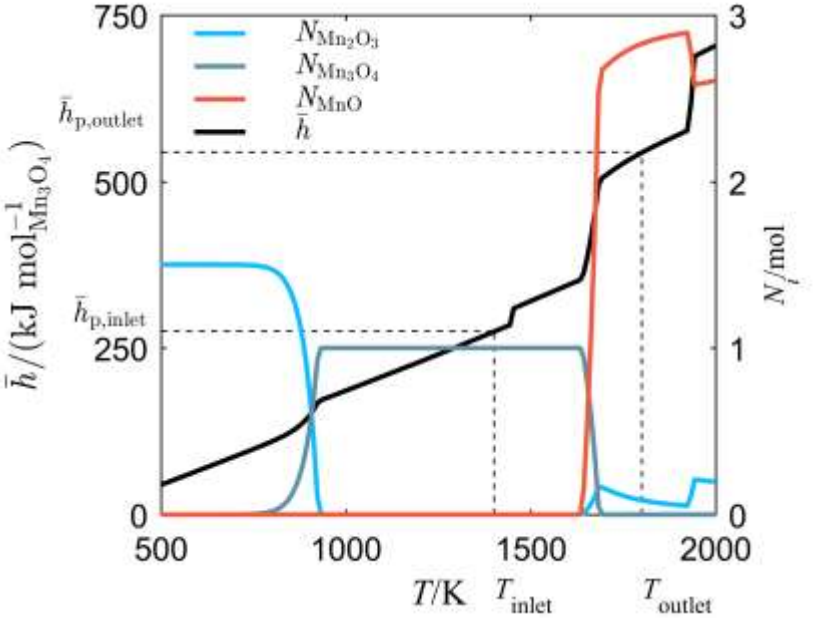


Fig 3. Molar specific enthalpy of the reactive mixture and amount of substance of mixture components.

$$\int_{\text{tube,inner}} h_{\text{tot}} \left(T_{\text{tube}} - T_{\text{flow}}\right) \mathrm{d}A = \dot{n}_{\text{p}} \left(\bar{h}_{\text{p,outlet}} - \bar{h}_{\text{p,inlet}}\right) + \dot{n}_{\mathrm{N_2}} \left(\bar{h}_{\mathrm{N_2,outlet}} - \bar{h}_{\mathrm{N_2,inlet}}\right) + \dot{n}_{\mathrm{O_2}} \bar{h}_{\mathrm{O_2,outlet}}$$

# Governing equations

- Fluidization [1]

$$h_{\mathrm{tot}} = \delta_{\mathrm{w}} h_{\mathrm{rad}} + 1.13\left[ k_{\mathrm{e}}^{\circ} \rho_{\mathrm{p}} \left(1-\varepsilon_{\mathrm{mf}}\right) c_{p,\mathrm{p}} n_{\mathrm{w}} \left(1-\delta_{\mathrm{w}}\right)\right]^{0.5}$$

$$\frac{u_{\mathrm{mb}}}{u_{\mathrm{mf}}} = \frac{2300 \rho_{\mathrm{g}}^{\,0.13} \mu^{0.52} \exp^{0.72 P_{45\mu\mathrm{m}}}}{d_{\mathrm{p}}^{\,0.8} \left(\rho_{\mathrm{p}} - \rho_{\mathrm{g}}\right)^{0.93}}$$

$$u_{\mathrm{mf}} = \frac{d_{\mathrm{p}}^{2}\left(\rho_{\mathrm{p}} - \rho_{\mathrm{g}}\right) g}{150\mu} \frac{\varepsilon_{\mathrm{mf}}^{3} \varphi_{\mathrm{s}}^{2}}{1-\varepsilon_{\mathrm{mf}}}$$

- Thermal stress

$$\sigma_{\mathrm{t}} = \frac{E\beta}{1-\nu} \frac{1}{r^2} \left( \frac{r^2 + r_{\mathrm{i}}^2}{r_{\mathrm{o}}^2 - r_{\mathrm{i}}^2} \int_{r_{\mathrm{i}}}^{r_{\mathrm{o}}} Tr\mathrm{d}r + \int_{r_{\mathrm{i}}}^{r} Tr\mathrm{d}r - Tr^2 \right)$$

$$\sigma_{\mathrm{r}} = \frac{E\beta}{1-\nu} \frac{1}{r^2} \left( \frac{r^2 - r_{\mathrm{i}}^2}{r_{\mathrm{o}}^2 - r_{\mathrm{i}}^2} \int_{r_{\mathrm{i}}}^{r} Tr\mathrm{d}r - \int_{r_{\mathrm{i}}}^{r} Tr\mathrm{d}r \right)$$

$$\sigma_{\mathrm{z}} = \frac{E\beta}{1-\nu} \left( \frac{2}{r_{\mathrm{o}}^2 - r_{\mathrm{i}}^2} \int_{r_{\mathrm{i}}}^{r_{\mathrm{o}}} Tr\mathrm{d}r - T \right)$$

$$\sigma_{\mathrm{v}} = \left[ \sigma_{\mathrm{t}}^2 + \sigma_{\mathrm{r}}^2 + \sigma_{\mathrm{z}}^2 - \left(\sigma_{\mathrm{t}}\sigma_{\mathrm{r}} + \sigma_{\mathrm{t}}\sigma_{\mathrm{z}} + \sigma_{\mathrm{r}}\sigma_{\mathrm{z}}\right)\right]^{0.5}$$

Reference:
[1] D. Kunii, O. Levenspiel, Fluidization Engineering, 2nd ed., Butterworth–Heinemann, Newton, 1991.

# Governing equations

- Initial and boundary conditions

$$T\left(t=t_0\right)=T_{\text{amb}}$$

$$-k_{\text{cond}}\nabla T\big|_{\text{cavity surfaces}}\cdot\hat{\mathbf{n}}=\varepsilon E_{\text{b}}-\alpha H=\varepsilon\sigma T^4+\alpha\int_{\Omega=0}^{2\pi}I\left(\hat{\mathbf{s}}_{\text{i}}\right)\hat{\mathbf{n}}\cdot\hat{\mathbf{s}}_{\text{i}}\,\mathrm{d}\Omega$$

$$-k_{\text{wall}}\nabla T\big|_{\text{wall,outer}}\cdot\hat{\mathbf{n}}=h_{\text{conv}}\left(T-T_{\text{amb}}\right)$$

$$-k_{\text{tube}}\nabla T\big|_{\text{tube,inner}}\cdot\hat{\mathbf{n}}=\begin{cases}0, & t<t_{\text{flow}}\\ h_{\text{tot}}\left(T-T_{\text{flow}}\right), & t\geq t_{\text{flow}}\end{cases}$$

$$T_{\text{flow}}=\begin{cases}T_{\text{ox}}=1400\text{ K} & \left(\text{Lower temperature bound}\right)\\ T_{\text{red}}=1800\text{ K} & \left(\text{Upper temperature bound}\right)\end{cases}$$

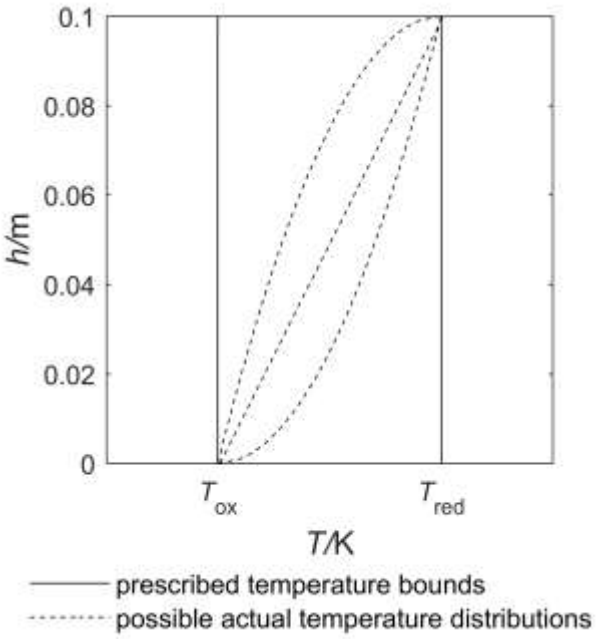


Fig 4. Assumed temperatures for the reactive flow.

# Numerical solutions

- Energy equation is discretised using the finite volume method in space and the explicit Euler scheme in time.
- Net flux on cavity surfaces calculated using energy-partitioning Monte Carlo ray-tracing.
- Programmed using Fortran 90 and CALC libraries.
- Nonconforming orthogonal mesh is applied to the reactor odd geometry.
- Adaptive time advancement is used to reduce the computational effort

- Converge criterion

$$\max\left(T_k^{i+1} - T_k^i\right) < 10^{-3}\,\mathrm{K},\ k \in [1, N]$$

- The results are independent from the mesh, ray number, and time advancement step.

# Results

## Safety—Peak temperature and thermal stress

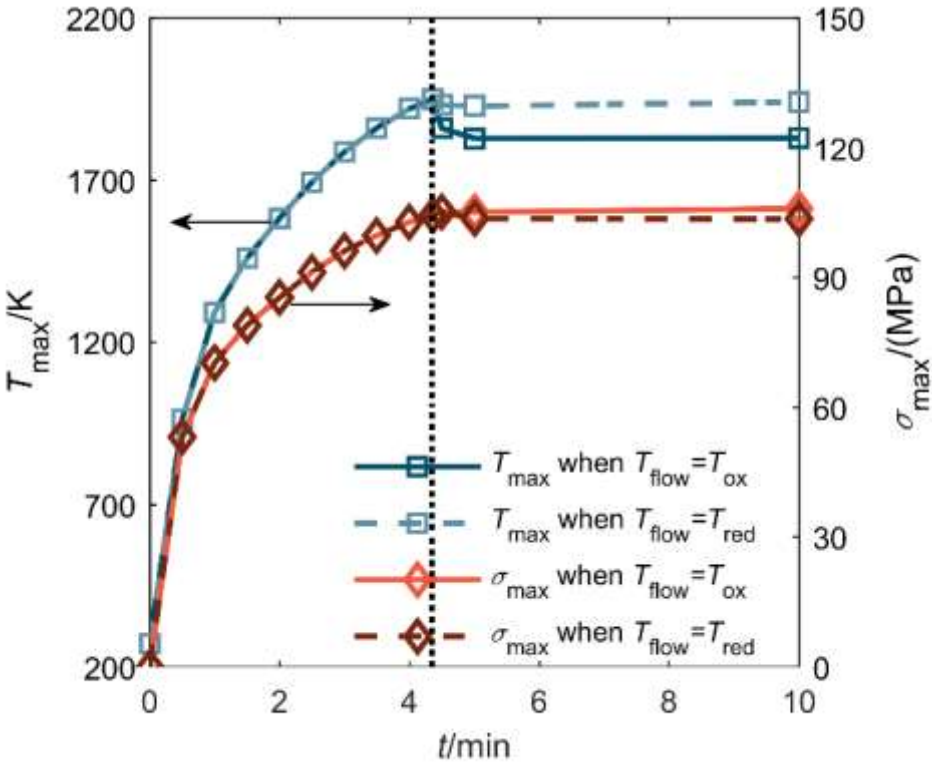


Fig 5. Peak temperature and thermal stress of the reactor tube.

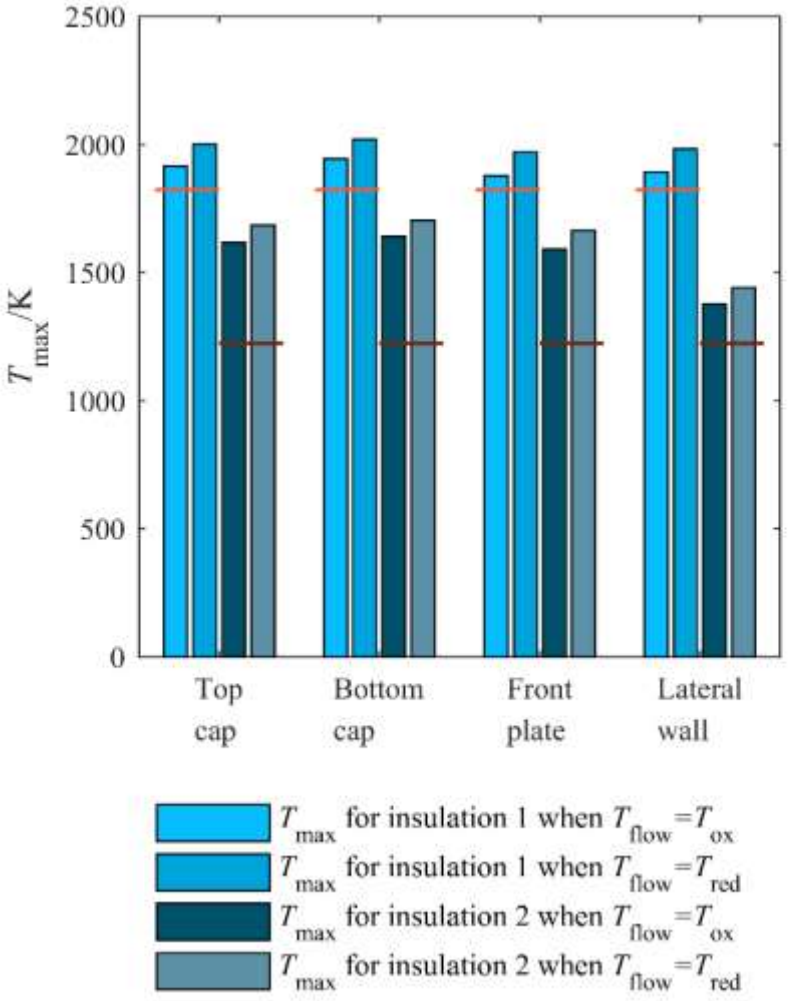


Fig 6. Maximum temperature in the reactor insulation layers with different assumed flow temperature.

# Results

## Safety—Location of hot spots

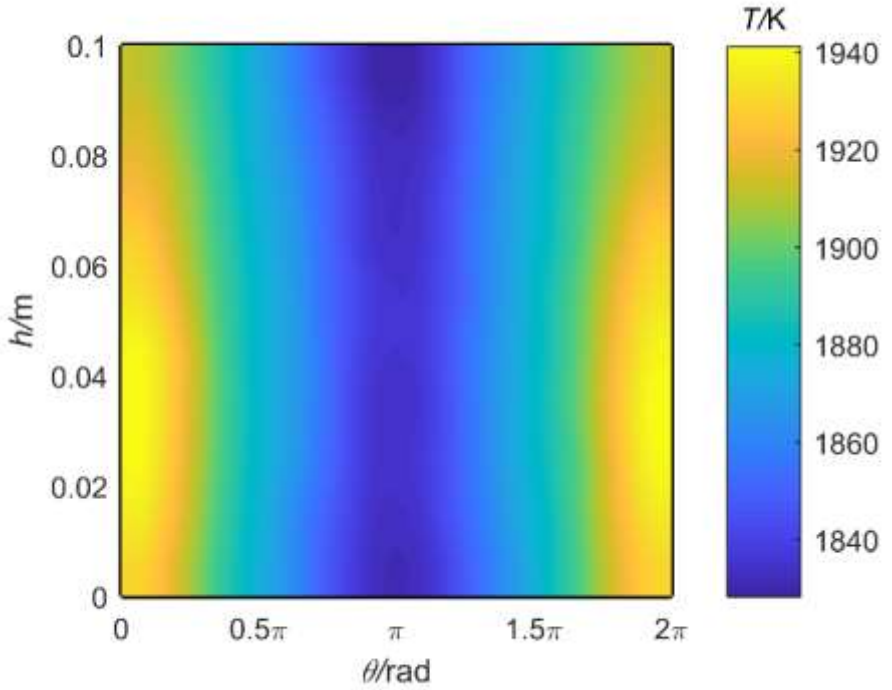


Fig 7. Temperature distribution on the reactor tube outer surface. The azimuthal angle of 0 and 2π represent the direction facing the aperture.

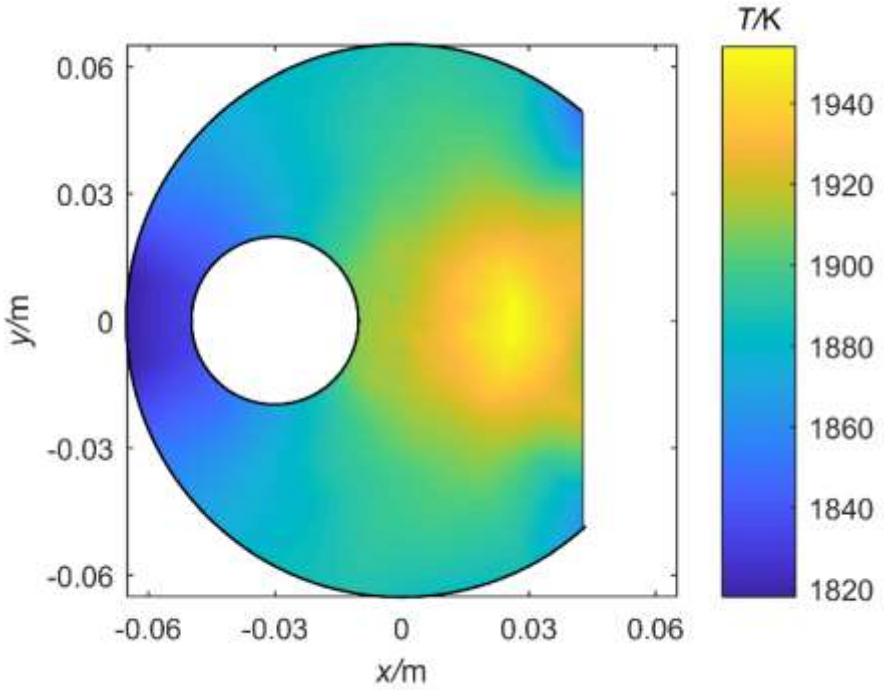


Fig 8. Temperature distribution on the cavity bottom surface.

# Results

Efficiency—Energy balance of the reactor

$$\gamma_i = \frac{Q_i}{C \cdot A \cdot \mathrm{DNI}}$$

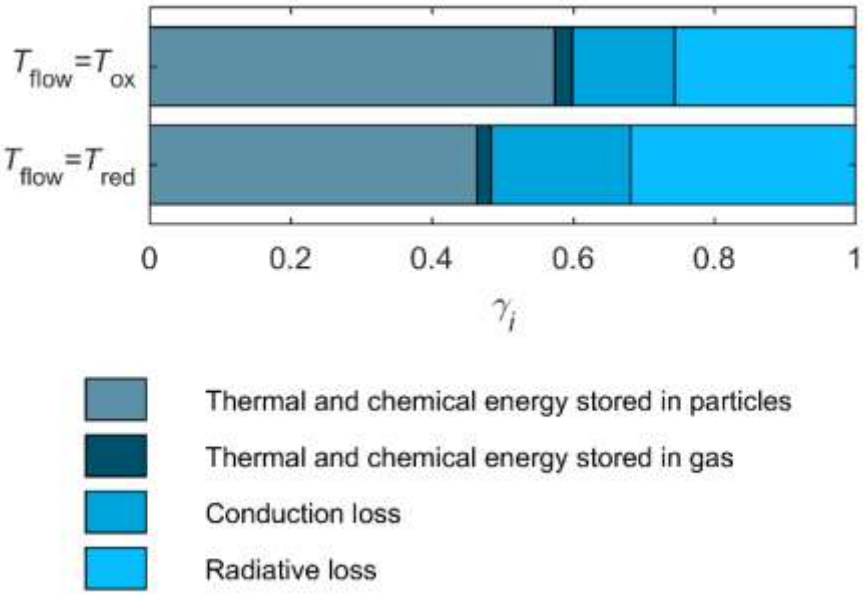


Fig 9. Energy balance of the reactor at steady state with different assumed flow temperatures.

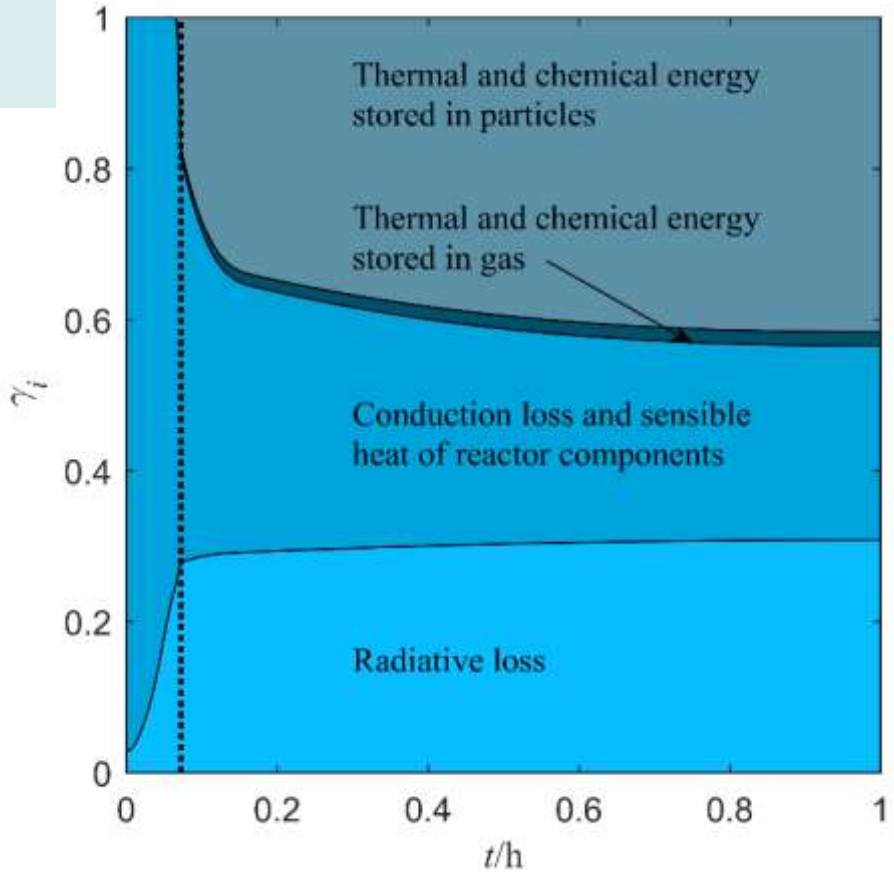


Fig 10. Instantaneous energy balance of the reactor.

# Results

## Effect of incident radiation directionality

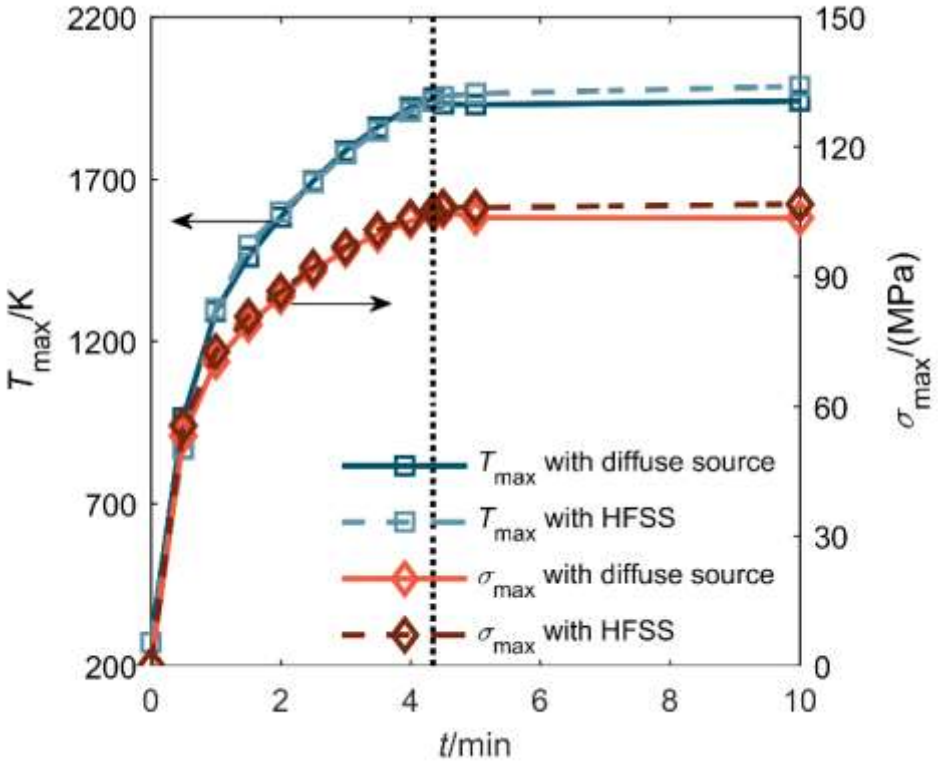


Fig 11. Maximum temperature and thermal stress in the reactor tube with different radiation sources.

# Conclusions

**Safety**

- The peak temperature of reactor tube and first layer of insulation (ZAL-15) slightly exceeds the allowable temperature. The peak temperature of the second layer of insulation (MICROSIL) exceeds the allowable temperature by 400 K.
- The thermal stress is well below the flexural strength of the materials.

**Efficiency**

- The solar-to-thermochemical efficiency is 46.3%–57.4%.
- $Mn_3O_4$ particles are reduced at the mass flow rate of 0.70–0.87 g $s^{-1}$.

**Effect of incident radiation directionality**

- The non-uniform flux distribution from the HFSS shows no notable differences from an ideal diffuse source in reactor peak temperature, thermal stress, and efficiency.

**Future work**

- Verification with comprehensive CFD model.
  - Conduction in insulation: pseudo 3-D ⟶ 3-D
  - Multiphase flow: semi-empirical model ⟶ Eulerian model
- Validation with experiment.

## Acknowledgement

Financial support by the Australian Renewable Energy Agency, grant no. 2014/RND005, is gratefully acknowledged.

## Contact

Corresponding author
Prof. Wojciech Lipiński
wojciech.lipinski@anu.edu.au

Presenter
Bo Wang
bo.wang@anu.edu.au

**Thanks for your attention!**